Wavelength and temperature dependence of the absolute O(^1D) production yield from the 305–329 nm photodissociation of ozone

Kenshi Takahashi, Nori Taniguchi,[a] and Yutaka Matsumi[b]
Solar Terrestrial Environment Laboratory and Graduate School of Science, Nagoya University, 3-13, Honohara, Toyokawa 442-8507, Japan

Masahiro Kawasaki
Department of Molecular Engineering, Kyoto University, Kyoto 606-8501, Japan

Michael N. R. Ashfold
School of Chemistry, University of Bristol, Bristol BS8 1TS, United Kingdom

(Received 22 December 1997; accepted 27 January 1998)

O(^1D) and O(^3P_j) photofragments produced in the photodissociation of ozone in the wavelength range 305–329 nm both at 295 and 227 K have been detected directly using a technique of laser induced fluorescence (LIF) in the vacuum ultraviolet (vuv). Photofragment excitation (PHOFEX) spectra for both species have been measured by scanning the photodissociation laser wavelength whilst monitoring vuv-LIF at 115 nm [O(^1D)] and 130 nm [O(^3P_j)]. After applying suitable corrections for the relative detection sensitivities, suitably weighted combinations of these PHOFEX spectra were found to provide a quantitative match to the parent O_3 absorption spectrum both at 295 and 227 K, thereby providing a method of determining both the wavelength and temperature dependence of the absolute O(^1D) quantum yield, $\Phi_{1D}(\lambda,T)$. Hot band excitation of internally excited O_3 molecules and dissociation via the spin-allowed channel yielding $O(^1D)+O_2(a\ ^1\Delta_g)$ products makes the dominant contribution to the quantum yield $\Phi_{1D}(\lambda,T)$ in the wavelength range 310–320 nm. For $\lambda>320$ nm, however, both the Doppler profiles of the nascent O(^1D) atoms and the temperature dependence of the O(^1D) yield indicate that the O(^1D) atoms must arise predominantly via the spin-forbidden channel yielding $O(^1D)+O_2(X\ ^3\Sigma_g^-)$. The analysis allows a first determination of the absolute branching to this channel ($\Phi\sim0.08$) following O_3 photolysis in the wavelength range 318–329 nm. The present work highlights remaining deficiencies in the latest NASA/JPL recommendations regarding the wavelength and temperature dependence of the O(^1D) yield resulting from O_3 photolysis at $\lambda>320$ nm. © *1998 American Institute of Physics.* [S0021-9606(98)01617-1]

I. INTRODUCTION

The near ultraviolet photochemistry of ozone remains a topic of great contemporary interest because of its pivotal role in establishing the oxidative capacity of the Earth's atmosphere. It has long been recognized that, simply on energetic grounds, no fewer than four different fragmentation pathways might contribute to the overall decay of ozone molecules following excitation in the all important UV wavelength region around 310 nm:

$$O_3+h\nu(\lambda\leqslant310\text{ nm})\rightarrow O(^1D)+O_2(a\ ^1\Delta_g), \quad (1)$$

$$O_3+h\nu(\lambda\leqslant411\text{ nm})\rightarrow O(^1D)+O_2(X\ ^3\Sigma_g^-), \quad (2)$$

$$O_3+h\nu(\lambda\leqslant611\text{ nm})\rightarrow O(^3P)+O_2(a\ ^1\Delta_g), \quad (3)$$

$$O_3+h\nu(\lambda\leqslant1180\text{ nm})\rightarrow O(^3P)+O_2(X\ ^3\Sigma_g^-), \quad (4)$$

where the long wavelength limits given in parentheses indicate the thermodynamic threshold for the various fragmentation pathways in the case that the parent ozone molecule is excited from its ground ($v''=0$) state.[1] Channel (1) dominates at $\lambda<310$ nm, with a reported quantum yield of ~0.9 throughout the intense Hartley band absorption (220–310 nm). Much recent interest[2–15] has focussed on possible contributions from the spin-forbidden fragmentation channels (2) and (3) and, in particular, on the various possible formation mechanisms for O(^1D) photoproducts following ozone photodissociation at $\lambda\geqslant310$ nm, i.e., below the energetic threshold for the spin-allowed process (1), since the formation of O(^1D) at $\lambda>310$ nm has direct impact on tropospheric OH radical concentrations.[16] Hancock and co-workers[5,7–9] investigated $O_2(a\ ^1\Delta_g)$ fragment formation following photoexcitation of O_3 within this long wavelength region, both by studying the temperature dependence of the $O_2(a\ ^1\Delta_g)$ yield and by time-of-flight (TOF) mass spectroscopy. Their studies show conclusively that both hot band excitation [and subsequent fragmentation via channel (1)] and dissociation via the spin-forbidden channel (3) contribute to the observed $O_2(a\ ^1\Delta_g)$ yield; partition function and Franck–Condon considerations dictate that the spin-forbidden process must become the main route to any $O_2(a\ ^1\Delta_g)$ product formation at the longest excitation wavelengths ($\lambda>320$ nm).

[a]On leave from Graduate School of Environmental Earth Science, Hokkaido University, Sapporo 060-0810, Japan.
[b]Author to whom correspondence should be addressed.

 © 1998 American Institute of Physics

Downloaded 18 Oct 2006 to 133.6.32.11. Redistribution subject to AIP license or copyright, see http://jcp.aip.org/jcp/copyright.jsp

As long ago as 1980, Brock and Watson[4] suggested that channel (2) was responsible for the observed production of $O(^1D)$ atoms following excitation of O_3 at energies below the threshold for channel (1), but it is only recently that the confirmatory experimental measurements have become available. The most compelling experimental data comes in the form of photofragment excitation (PHOFEX) spectra for production of $O(^1D)$ atoms following O_3 photolysis in the bulk at 298 and at 227 K, and in a supersonic molecular beam.[10–13] The room temperature PHOFEX spectrum in the range 308–326 nm shows a smooth, apparently unstructured variation in the $O(^1D)$ signal with photolysis laser wavelength, which is attributable to spin allowed-photodissociation [process (1)] of the small percentage of vibrationally excited ozone molecules present in a 298 K sample.[10,13] Analysis of the PHOFEX spectrum suggests that prior excitation in the ν_3 (asymmetric stretching mode) is most efficacious in promoting the fragmentation process.[12] This ''hot band'' contribution becomes progressively less significant as the sample temperature is reduced to the extent that the jet-cooled PHOFEX spectrum for forming $O(^1D)$ atoms shows well resolved structure[10–12] which mimics the known[17,18] vibronic structure of the Huggins band of ozone. $O(^1D)$ Doppler line shape analysis[12] confirms that these $O(^1D)$ atoms arise from excitation of vibrationally ground state O_3 molecules and subsequent fragmentation via the spin-forbidden pathway (2). In this paper we report detection of both $O(^3P)$ and $O(^1D)$ atoms by vacuum ultraviolet laser induced fluorescence (vuv-LIF) following photolysis of flowing ozone samples over the wavelength range 305–329 nm, both at room temperature and at 227 K. Comparing these PHOFEX spectra with the parent absorption spectrum (recorded at the appropriate temperature)[19,20] allows determination of the wavelength dependence of the absolute quantum yields for forming $O(^3P)$ and $O(^1D)$ atoms at 295 and 227 K. Companion studies, at a number of user selected wavelengths, of the way in which the respective yields vary over the temperature range 227–298 K demonstrate a clear means of distinguishing the relative contributions that spin-allowed fragmentation of vibrationally 'hot' ozone molecules and the spin-forbidden dissociation (2) each make to the overall $O(^1D)$ product yield. The present findings serve to reinforce the need for further revision of the long wavelength part of the NASA/JPL recommendations[2] regarding the quantum yield curve for $O(^1D)$ atom formation in the near ultraviolet photodissociation of ozone.

II. EXPERIMENT

The experimental arrangement and procedures are essentially the same as in our previous studies of ozone photolysis.[6,10] Ozone was prepared by passing ultra-pure O_2 (Nihon Sanso, 99.9995%) through a commercial ozonizer and trapping the product on cooled silica gel. The product was degassed at liquid N_2 temperature and stored in a blackened glass bulb. O_3 (5% mixture in Ar) was flowed into the reaction chamber through glass tubing and a needle valve made of poly-tetra fluoro ethylene. The sample gas temperature was varied, over the range 227–298 K, by surrounding the final stage of the gas delivery system with a jacket containing a dry-ice–methanol slush. This same slush mixture was used to cool a simple copper radiation shield (equipped with appropriate apertures for passing the pump and probe laser beams) mounted around the interaction region in the chamber. The gas temperature was measured using a fine thermocouple located just downstream of the photodissociation region. The chamber is evacuated by a rotary pump (Alcatel, 2520, 330 ℓ/min) through a liquid N_2 trap, and maintained at a total pressure of 1 Torr as measured by a capacitance manometer (MKS, Baratron 220, 2 Torr full span).

The photolysis radiation, tunable over the range 305–329 nm, was generated using a Nd:YAG laser pumped dye laser operating at 10 Hz repetition rate with a mixture of DCM and Sulforhodamine 101 dyes, and subsequent frequency doubling using a KD*P crystal mounted in an autotracking system (Spectra Physics GCR-190, PDL-3 and WEX-2, respectively). The bandwidth of the uv radiation was $\sim 0.2\ cm^{-1}$ (FWHM). Wavelength calibration, in the visible, was achieved by measuring the fluorescence excitation spectrum of iodine vapor and comparing it with published data.[21] The required second harmonic radiation was isolated using a uv transmitting filter (Toshiba, UVD33S). A photodiode (itself calibrated against a Scientech, AC50UV laser power meter) was used to monitor the uv photodissociation pulse intensity throughout each experiment in order to allow subsequent normalization of the photofragment vuv-LIF signal intensities. The uv output had an energy of ~ 1 mJ/pulse, varying by only $\sim 20\%$ over the entire 305–329 nm wavelength range, and a beam diameter in the interaction region of ~ 4 mm.

The $O(^3P_j)$ and $O(^1D)$ photoproducts were both detected by vacuum ultraviolet laser induced fluorescence (vuv-LIF). The former are monitored most conveniently via the $3s\ ^3S^0-2p\ ^3P_j$ transition at ~ 130 nm (130.22, 130.48 and 130.60 nm for $j=2$, 1 and 0, respectively). The necessary vuv radiation was generated by two photon resonant four-wave difference frequency mixing $(2\omega_1-\omega_2)$ in krypton gas (14 Torr), using two tunable dye lasers pumped simultaneously by an XeCl excimer laser (two Lambda Physik FL3002's and Lextra-50). The output of one dye laser (operating with Bis-MSB dye in 1,4-dioxane) was frequency-doubled using a BBO crystal to yield $\lambda_1=212.56$ nm, which is two photon resonant with the $5p[1/2]_0-{}^1S_0$ transition of Kr. The second dye laser was operated with Coumarin 540A in methanol solution to generate $\lambda_2=578.1$, 572.8, and 570.6 nm which, when mixed with two ω_1 photons, correspond to the appropriate vuv frequencies for detecting $O(^3P_j)$ atoms with $j=2$, 1, and 0, respectively. $O(^1D)$ atoms were detected by vuv-LIF on the $3s\ ^1D^0-2p\ ^1D$ transition at 115.22 nm. Radiation at this wavelength was generated by phase-matched frequency tripling of the output from a single XeCl pumped dye laser (operating on PTP in 1,4-dioxane at 345.6 nm, ~ 5 mJ incident pulse energy) in a xenon (40 Torr)/argon (160 Torr) gas mixture.[22]

The laser beam(s) for the four-wave difference mixing or frequency tripling were focused ($f=200$ mm fused silica lens) into a stainless steel cell containing Kr or Xe/Ar gas and emerged, along with the generated vuv radiation,

Downloaded 18 Oct 2006 to 133.6.32.11. Redistribution subject to AIP license or copyright, see http://jcp.aip.org/jcp/copyright.jsp

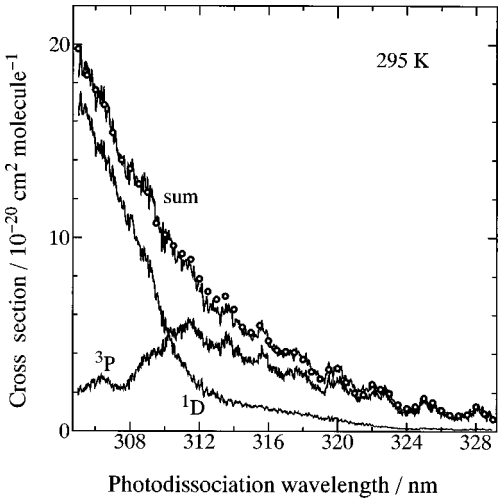

FIG. 1. Photofragment excitation (PHOFEX) spectra for O(^3P) and O(^1D) photofragments recorded at 295 K together with their sum spectrum. The open circles are O_3 absorption cross sections at 295 K reported by Malicet *et al.* (Ref. 20). The horizontal axis represents the wavelength of the uv photodissociation laser, whilst the vertical scale is for the absorption cross section. Scaling factors for the individual PHOFEX spectra are determined so that the sum spectrum fits the absorption cross sections shown by open circles (see the text).

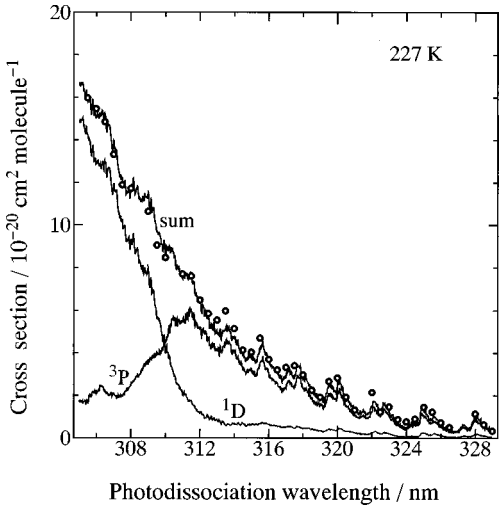

FIG. 2. Photofragment excitation (PHOFEX) spectra for O(^3P) and O(^1D) photofragments recorded at 227 K along with their sum spectrum. Open circles are O_3 absorption cross sections at 228 K reported by Malicet *et al.* (Ref. 20). The horizontal axis represents the wavelength of the uv photodissociation laser, and the scaling for the vertical axes are similar to that in Fig. 1.

through an LiF window into the reaction chamber where it collinearly counterpropagated with the photolysis beam. Another LiF window mounted in the chamber beyond the photodissociation region reflected part of the probe laser pulse towards a vuv monochromator, and the intensity of transmitted vuv radiation was monitored using a solar-blind photomultiplier tube (Hamamatsu, R1259). The delay time between the photolysis and probe laser pulses was controlled by a pulse generator (Stanford Research, DG535) and typically set at 50–60 ns (but could be extended to as long as 25 μs) with a jitter of <10 ns.

The vuv-LIF signals associated with both the O(^1D) and the O(^3P_j) photoproducts were detected along the vertical axis, orthogonal to propagation direction of both vuv probe and photodissociation laser beams, using a solar blind photomultiplier tube (EMR, 541J-08-17) equipped with an LiF window and a KBr photocathode sensitive only to radiation in the wavelength range 105–150 nm. This fluorescence detection direction is parallel to ϵ_{phot}, the electric vector of the uv photodissociation radiation, and perpendicular to ϵ_{probe}, the electric vector of the vuv probe laser. The output of the photomultiplier was preamplified and averaged over 10 laser pulses using a gated integrator (Stanford, SR-250). Given that the PHOFEX spectra for both O(^1D) and O(^3P_j) atoms were recorded whilst scanning the wavelength of the uv photolysis laser at 0.0075 nm/s we estimate the actual resolution of the PHOFEX spectra to be ~ 1 cm^{-1}. We emphasize the fact that the extreme sensitivity of the vuv-LIF technique allows detection of O(^1D) and O(^3P_j) atoms at such low O_3 pressures and at such short pump–probe delay times and signal integration times that secondary reactions—even, for example, the reaction of O(^1D) atoms with O_3 molecules, which occurs at the gas kinetic collision rate ($k=1.2$–2.8×10^{-10} cm^3 molecule^{-1} s^{-1})[2,15]—can safely be ignored.

III. RESULTS

A. Determination of the wavelength dependence of the absolute O(^1D) production yield from the photodissociation of ozone

Figures 1 and 2 show PHOFEX spectra of the O($^3P_2$) and O(^1D) photoproducts recorded over the range 305–329 nm at a gas temperature of 295 and 227 K, respectively. These were obtained by scanning the photodissociation laser wavelength and monitoring the resulting resonance fluorescence when the wavelength of the probe vuv laser was fixed at the center of, respectively, the $3s^3S^0-2p\ ^3P_2$ resonance line at 130.22 nm and the $3s\ ^1D^0-2p\ ^1D$ transition at 115.22 nm. The total pressure in the interaction region was 30 mTorr, of which 10% was O_3, and the pump–probe time delay was 50 ns. As previously,[10] checks were made (at photolysis wavelengths of 305, 308, 312, and 322 nm) to ensure that the LIF signal scaled linearly with the intensity of the uv photodissociation laser pulse (Fig. 3). In both cases the raw experimental PHOFEX spectrum has been corrected for variations in the intensities of both the photodissociation and vuv probe laser intensities (photons/pulse).

Various factors need to be considered before any quantitative analysis of either PHOFEX spectrum. Consider first the PHOFEX spectrum for forming O($^3P_2$) atoms. For it to be a valid measure of the *total* O(^3P) yield we need to establish the wavelength dependence of the fine-structure populations among the j levels of the O(^3P_j) atoms produced from the photodissociation of O_3. This was checked, as before,[6,10] by scanning the vuv probe laser wavelength at a number of (fixed) photodissociation wavelengths and recording the excitation spectrum of the O(^3P_j) atoms at both 227 and 295 K. Relative sensitivity factors for the three $3s^3S^0-2p\ ^3P_j$ transitions were obtained by comparing the three peak areas recorded at long time delays (20 μs, corresponding to a fully thermalized fine-structure population dis-

Downloaded 18 Oct 2006 to 133.6.32.11. Redistribution subject to AIP license or copyright, see http://jcp.aip.org/jcp/copyright.jsp

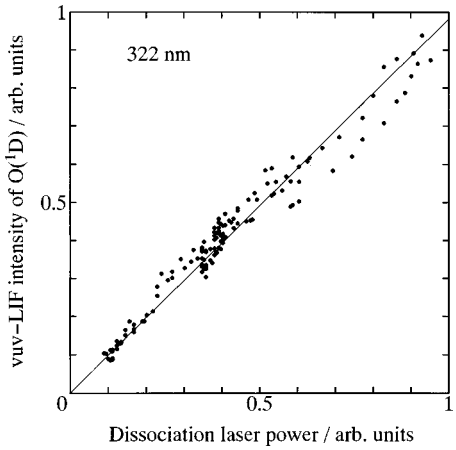

FIG. 3. Photodissociation laser power dependence of the vuv laser-induced fluorescence signal for the $O(^1D)$ photofragments resulting from ozone photodissociation at 322 nm. Fluorescence is detected on the $3s\ ^1D^0-2p\ ^1D$ transition at 115.215 nm. The straight line shows the best fit from a least squares fitting of the data points. The O_3 pressure was 4 mTorr and the time delay between the photodissociation and vuv probe beams was 60 ns.

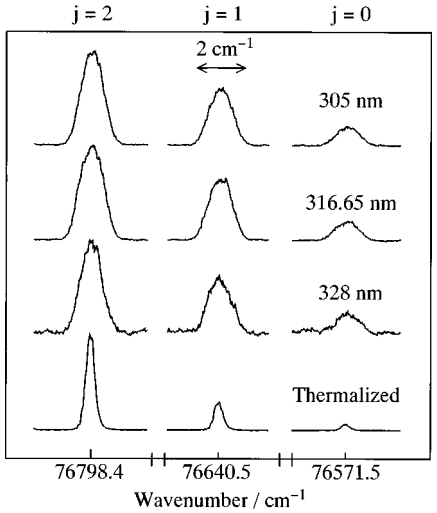

FIG. 4. Vacuum ultraviolet laser-induced fluorescence spectra for $O(^3P_j$, $j=2,1,0)$ photofragments from the photodissociation of O_3 at three different wavelengths at 227 K. The horizontal axis shows the wave number of the vuv probe laser light. The O_3 pressure was 3 mTorr for each of the three upper panels and the time delay between the photodissociation and vuv probe laser pulses was 50 ns. The thermalized spectra shown in the bottom panel were measured with 2 mTorr of O_3 in 1.5 Torr of Ar buffer gas, a dissociation laser wavelength of 305 nm, and a time delay between the photolysis and probe laser pulses of 20 μs. All results are normalized against the intensity of the vuv probe laser light. The vertical scaling has been chosen so that the height of the $O(^3P_2)$ line shape is the same in each panel.

tribution) with the corresponding population ratios predicted through use of the Boltzmann equation. These sensitivity factors were then applied to the relative peak areas measured in excitation spectra taken at short (50 ns) time delays in order to derive the nascent $O(^3P_j)$ spin–orbit state population ratios. Results obtained at 227 K for three photodissociation wavelengths (305 nm, 312 nm and 328 nm) are results are listed in Table I. Key points to note are: (i) the values obtained at the three different photodissociation wavelengths are the same within experimental error, i.e., there is no discernable change in the fine-structure branching ratio within the range of photodissociation wavelengths considered here; (ii) the values obtained here at a sample temperature of 227 K are the same, within experimental error, as those found earlier[6,10] at 295 K at other photodissociation wavelengths within the same range, i.e., there is no discernable temperature dependence to the $O(^3P_j)$ fine-structure branching ratio. As a final check, we recorded the PHOFEX spectrum for forming $O(^3P_1)$ atoms from the photodissociation of O_3 at 295 K over the same 305–329 nm wavelength range. It is identical in appearance to that shown in Fig. 1 and from hereon we assume that measurements involving $O(^3P_2)$ atoms provide a faithful indication of the behavior of the complete $O(^3P)$ atom yield.

TABLE I. Fine-structure branching ratios of the $O(^3P_j)$ atoms produced from the photodissociation of O_3 in the wavelength range 305–328 nm.

λ_{phot}[a]	T[b]	$N_{j=2}$	$N_{j=1}$	$N_{j=0}$
305.0	227	0.60±0.02	0.31±0.02	0.10±0.01
312.0	227	0.62±0.02	0.30±0.02	0.09±0.01
328.0	227	0.62±0.02	0.30±0.02	0.09±0.01
Boltzmann	227	0.788	0.174	0.037
308.0[c]	295	0.65±0.02	0.27±0.02	0.08±0.01
316.0[c]	295	0.63±0.03	0.28±0.02	0.09±0.01
324.0[c]	295	0.63±0.02	0.28±0.02	0.09±0.01
Boltzmann	295	0.741	0.209	0.050
Statistical[d]		0.555	0.333	0.111

[a]Photodissociation wavelengths in units of nm.
[b]Sample gas temperature in units of K.
[c]Taken from Reference 10.
[d]Degeneracy ratios, $(2j+1)$.

A second factor also needs to be considered. The exoergicity of process (4) ensures that the $O(3s\ ^3S^0-2p\ ^3P_j)$ transitions have Doppler widths, $\Delta\nu_{1D}$, comparable to the probe laser bandwidth.[6] The PHOFEX spectrum shown in Fig. 1 was obtained by setting the probe laser wavelength at the center of the $O(3s\ ^3S^0-2p\ ^3P_2)$ lineshape. Such a PHOFEX spectrum will only give a faithful indication of the total $O(^3P)$ atom yield if the Doppler lineshape remains constant across the 305–329 nm wavelength range. Figure 4 shows Doppler lineshapes of the nascent $O(^3P_j)$ atoms produced via O_3 photodissociation at 305.0 315.65, and 328.0 nm with, in each case, ϵ_{phot} perpendicular to k_{probe} (the propagation axis of the probe laser), together with a lineshape measured for a thermalised sample of $O(^3P)$ atoms at long (20 μs) time delay. The latter provides a measure of the experimental resolution, $\sim 0.82\ cm^{-1}$ (FWHM, modelled as a Gaussian), where no intracavity etalon was installed into the dye laser for vuv generation. Parent thermal motion at 227 K will contribute a Doppler spread of $0.2\ cm^{-1}$, thus we deduce the bandwidth of the 130 nm probe radiation to be $\sim 0.79\ cm^{-1}$ (FWHM). We confirm that to within the available resolution the experimental line shape remains constant across the 305–329 nm wavelength range. We comment here that Ball *et al.*[9] have measured the kinetic energy release of the $O_2(a\ ^1\Delta_g)$ photofragments resulting from O_3 photodissociation in the wavelength range 280–331 nm, and found that the $O_2(a\ ^1\Delta_g)$ fragments produced at $\lambda_{phot}>320$ nm

Downloaded 18 Oct 2006 to 133.6.32.11. Redistribution subject to AIP license or copyright, see http://jcp.aip.org/jcp/copyright.jsp

have higher kinetic energies than those formed via photodissociation at shorter wavelengths. They attributed this to dissociation via the spin-forbidden channel (3). The *maximum* recoil velocity that the resulting $O(^3P_j)$ atoms could have is $\sim 3800\ ms^{-1}$ assuming $\lambda_{phot}=320$ nm and that the $O_2(a\ ^1\Delta_g)$ partner fragments are formed in their vibrationless and rotationless level. Detailed kinetic energy and/or internal energy distributions for the products resulting from channel (3) have yet to be reported, but it is quite possible that the $O(^3P)$ atoms generated with $O_2(a\ ^1\Delta_g, v''=0, J''=0)$ cofragments could have larger kinetic energies than those formed in association with $O_2(X\ ^3\Sigma_g^-)$ fragments if the latter carry high internal energies. As Fig. 4 shows, we can discern no obvious variation in the $O(3s\ ^3S^0-2p\ ^3P_2)$ line shape or FWHM linewidth over the photodissociation wavelength range 305–329 nm. Thus we conclude that PHOFEX spectra such as that shown in Fig. 1, recorded with the probe laser wavelength fixed at the $O(3s\ ^3S^0-2p\ ^3P_2)$ line center can provide an accurate reflection of the photodissociation wavelength dependence of the total $O(^3P)$ yield.

The effects of Doppler broadening also need to be considered carefully when interpreting the $O(^1D)$ PHOFEX spectra shown in Figs. 1 and 2. We have shown previously[11] that the Doppler profiles of $O(^1D)$ fragments resulting from photolysis of jet-cooled O_3 molecules show a marked sensitivity to the parent excitation wavelength; $O(^1D)$ atoms resulting from the spin-forbidden predissociation (2), most evident at $\lambda_{phot}>315$ nm, exhibit significantly broader Doppler profiles than the $O(^1D)$ atoms arising via hot band excitation and the spin-allowed dissociation (1). Since Δv_{1D} exceeds the vuv probe laser linewidth, it is necessary to correct the $O(^1D)$ PHOFEX spectrum obtained by exciting at the line center of the $3s^1D^0-2p\ ^1D$ transition to allow for the wavelength dependence of the probe sampling efficiency. Thus it was necessary to record Doppler spectra of the $O(^1D)$ fragments resulting from O_3 photodissociation at both 295 and 227 K at many different excitation wavelengths. We measured the Doppler profiles of the nascent $O(^1D)$ photofragments at various photodissociation wavelengths in the range of 305–329 nm under the same experimental conditions as for the PHOFEX measurements at 295 and 227 K. Above $\lambda_{phot}\sim 310$ nm, the measured linewidths increase smoothly with increasing wavelength reflecting the fact that, on energetic grounds, the slow atoms from channel (1) must make a smaller and smaller contribution to the total $O(^1D)$ yield. Thus, unlike the case for the $O(^3P)$ yield considered above, the photodissociation wavelength dependent Doppler broadening of the $O(^1D)$ resonance line means that the $O(^1D)$ PHOFEX spectrum obtained simply by setting the vuv probe laser at the line center of the $O(3s\ ^1D^0-2p\ ^1D)$ transition does not give an accurate measure of the $O(^1D)$ yield. The $O(^1D)$ PHOFEX spectra shown in Figs. 1 and 2 are derived as follows: each point in the raw experimental spectrum is first normalized with respect to both the pump and probe laser intensities, and then further corrected by a scaling factor proportional to the effective excitation linewidth appropriate for that particular wavelength. For example, compensating for this wavelength dependent Doppler broadening requires that the intensity of the $O(^1D)$ PHOFEX spectra at $\lambda_{phot}=328$ nm has to be scaled by a factor of 1.25 and 1.56 relative to the signal intensity recorded at 305 nm for 227 and 295 K, respectively. Doppler profiles recorded with a higher resolution probe laser equipped with an intra-cavity etalon will be described later.

Having established that the various PHOFEX spectra provide reliable measures of the wavelength dependence of the $O(^1D)$ and $O(^3P_j)$ atom yields, it should be possible to place these spectra on an *absolute* scale by requiring that the sum of the two PHOFEX spectra equates to the absorption spectrum of the O_3 molecule recorded at the same sample temperature. Such a procedure is valid given that the photodissociation quantum yield of O_3 is essentially unity in this wavelength range. As before,[9] we require that

$$\sigma_{abs}(\lambda,T)=\sigma_{1D}(\lambda,T)+\sigma_{3P}(\lambda,T)$$
$$=s_{1D}Y_{1D}(\lambda,T)+s_{3P}Y_{3P}(\lambda,T), \quad (5)$$

where $\sigma_{abs}(\lambda,T)$ is the O_3 absorption cross section at wavelength λ and temperature T taken from Malicet *et al.*,[20] and $\sigma_{1D}(\lambda,T)$ and $\sigma_{3P}(\lambda,T)$ are the (temperature dependent) partial cross sections for O_3 absorbing and dissociating to form $O(^1D)$ and $O(^3P_j)$ atoms, respectively. $Y_{1D}(\lambda,T)$ and $Y_{3P}(\lambda,T)$ are the experimentally obtained photofragment yield spectra of $O(^1D)$ and $O(^3P_j)$ at temperature T, and s_{1D} and s_{3P} are adjustable coefficients reflecting the different detection sensitivities for $O(^1D)$ and $O(^3P_j)$ atoms, respectively. As Figs. 1 and 2 show, it is possible to obtain very satisfactory replications of the O_3 absorption spectrum throughout the wavelength range 305–329 nm at both 227 and 295 K simply by summing the relevant PHOFEX spectra each weighted with an appropriate choice of sensitivity coefficient. The uncertainties on the partial cross sections for $O(^3P_j)$ and $O(^1D)$ atom formation from O_3 photolysis over the entire 305–329 nm wavelength range are about $\pm 9\%$ as estimated from consideration of run-by-run fluctuations of, first, the yield spectrum measurements and, second, the fitting errors of the sensitivity coefficients in Eq. (5).

Given Figs. 1 and 2 we can derive the wavelength dependent quantum yield for forming $O(^1D)$ atoms from O_3 photodissociation at 227 and at 295 K using the expression

$$\Phi_{1D}(\lambda,T)\equiv\sigma_{1D}(\lambda,T)/[\sigma_{1D}(\lambda,T)+\sigma_{3P}(\lambda,T)]$$
$$=s_{1D}Y_{1D}(\lambda,T)/[s_{1D}Y_{1D}(\lambda,T)+s_{3P}Y_{3P}(\lambda,T)], \quad (6)$$

where $\Phi_{1D}(\lambda,T)$ is the quantum yield of $O(^1D)$ produced from O_3 photodissociation at the wavelength λ and temperature T. Figures 5 and 6 show the wavelength dependence of the $O(^1D)$ quantum yield so derived for both temperatures, together with the current JPL/NASA yield curve recommendations for use in stratospheric modelling.[2] The uncertainties in the present quantum yield values are estimated to be $\pm 15\%$ of the actual yield values. As commented previously,[10] the PHOFEX spectra for forming $O(^1D)$ atoms in the photolysis of O_3 are smooth in this wavelength range, whilst the $O(^3P)$ PHOFEX spectra carry the vibrational signatures associated with the Huggins band system of O_3. As a result, small dips are evident in both the $O(^1D)$ quantum

Downloaded 18 Oct 2006 to 133.6.32.11. Redistribution subject to AIP license or copyright, see http://jcp.aip.org/jcp/copyright.jsp

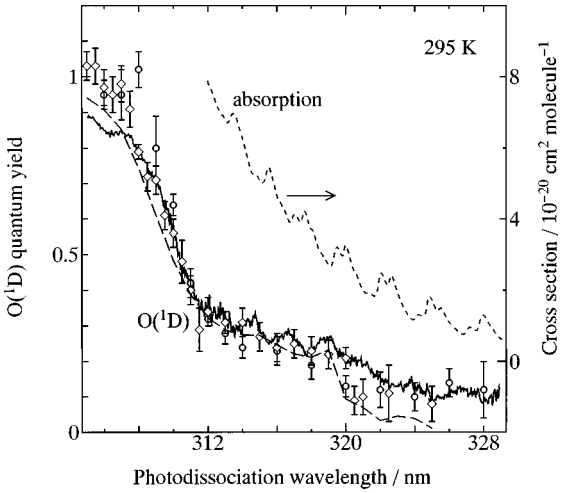

FIG. 5. The $O(^1D)$ quantum yield from the photodissociation of ozone at 295 K plotted as a function of dissociation wavelength. The dashed line shows the absorption spectrum of ozone at 295 K, reported by Malicet *et al.* (Ref. 20), offset vertically for clarity. Data points shown by the open circles are from Ball *et al.* (Ref. 13), and those indicated by the open rhombuses are from Trolier and Wiesenfeld (Ref. 3). The broken line shows the latest NASA/JPL recommendation (Ref. 2) for the wavelength dependent $O(^1D)$ quantum yield from O_3 photolysis at 295 K.

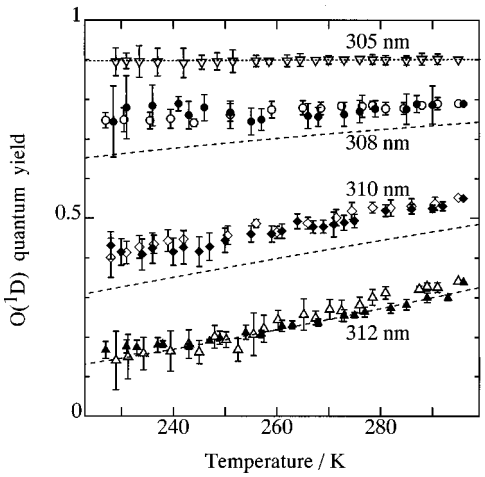

FIG. 7. Measured Φ_{1D} as a function of T (227–295 K) for $\lambda_{phot}=305$, 308, 310 and 312 nm. Data points obtained by monitoring $O(^1D)$ atoms are shown as open symbols, and those for $O(^3P_2)$ atoms by filled symbols. Both photoproducts were detected directly via the vuv-LIF technique. Both the time delay between the photodissociation laser light and vuv probe laser (60 ns) and the pressure of ozone (4 mTorr) were kept constant throughout the experiments. The broken lines show the current NASA/JPL recommendation at each wavelength (Ref. 2).

yield curves shown in Figs. 5 and 6 at each wavelength where these vibronic maxima occur. As Fig. 5 demonstrates, the present room temperature $O(^1D)$ quantum yield measurements are in good accord with those reported in our previous study at 298 K,[10] with the recent direct measurements of Ball *et al.*[13] and with the earlier data of Trolier and Wiesenfeld,[3] although the various results appear to show some small discrepancies at wavelengths ~305–306 nm. Experiments analogous to those reported here, but involving $O(^1D)$ and $O(^3P)$ atom detection following O_3 photolysis in the wavelength range 270–305 nm are now underway in our laboratory.

Also plotted in Fig. 6 are the $O_2(a\ ^1\Delta_g)$ photofragment yields measured by Ball *et al.* at 227 K.[8] This serves to reinforce the striking similarity between the quantum yield curves for forming $O(^1D)$ atoms and $O_2(a\ ^1\Delta_g)$ fragments, at least for $\lambda_{phot} \leqslant 322$ nm, that has been noted previously at 295 K.[13]

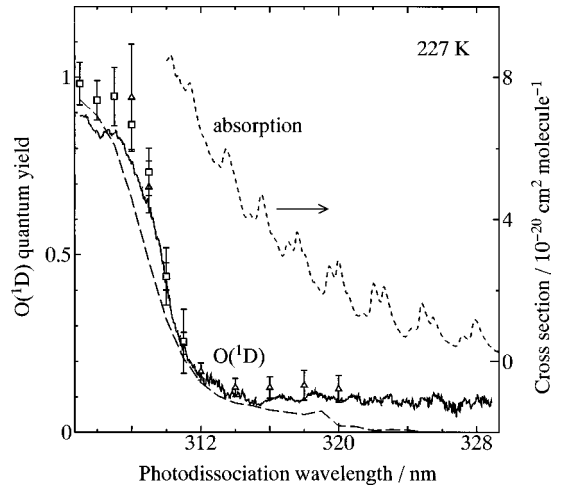

FIG. 6. The $O(^1D)$ quantum yield from the photodissociation of ozone at 227 K plotted as a function of dissociation wavelength. Separated results marked with open triangles and squares were reported by Ball *et al.* (Ref. 8) The absorption spectrum of ozone at 228 K, obtained by Malicet *et al.* (Ref. 20) is also shown (dashed line), offset vertically for clarity. The broken line is the latest recommendation by NASA/JPL (Ref. 2) for the wavelength dependent $O(^1D)$ quantum yield from O_3 photolysis at 227 K for use in stratospheric modelling.

B. Temperature dependence of the absolute $O(^1D)$ quantum yield from the photodissociation of ozone

Figures 7 and 8 illustrates in more detail how the $O(^1D)$ quantum yield from ozone photodissociation varies as a function of temperature for a number of selected wavelengths in the range 305–325 nm. The pressure of sample gas in the reaction cell was maintained constant throughout. All bar the 305 nm data in Fig. 7 were derived by monitoring

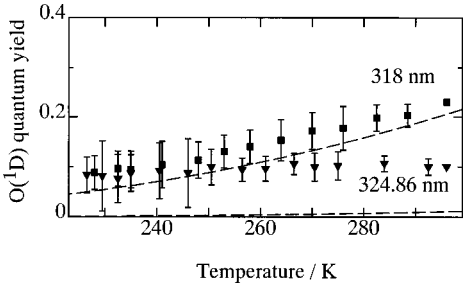

FIG. 8. Measured Φ_{1D} as a function of T (227–295 K) for $\lambda_{phot}=318$ and 324.86 nm. $O(^3P_2)$ atoms were detected directly via their vuv-LIF and the plotted $O(^1D)$ quantum yields are derived as $(1-\Phi_{3P}(\lambda,T))$—see the text. The broken lines show the current NASA/JPL recommendation (Ref. 2) for the temperature dependence of Φ_{1D} at each wavelength for use in stratospheric modeling.

Downloaded 18 Oct 2006 to 133.6.32.11. Redistribution subject to AIP license or copyright, see http://jcp.aip.org/jcp/copyright.jsp

both $O(^1D)$ and $O(^3P_2)$ atoms, whilst that shown in Fig. 8 comes from measurement of $O(^1D)$ atom yields only. Each plot was obtained by selecting a photodissociation wavelength and monitoring the vuv-LIF signal of the $O(^1D)$ or $O(^3P_2)$ atoms whilst gradually changing the gas temperature. Again, a number of correction factors need to be applied in order to equate the measured signal strengths with absolute quantum yields. Consider first the $O(^1D)$ data sets (open symbols) in Fig. 7. The signal $S_{1D}(\lambda,T)$ recorded at a chosen photodissociation wavelength λ as a function of temperature T was normalized with respect to both photodissociation and vuv probe laser pulse intensities, and then scaled as follows to give the required $O(^1D)$ quantum yield:

$$\Phi_{1D}(\lambda,T)=\Phi_{1D}(\lambda,295)\times\frac{S_{1D}(\lambda,T)}{S_{1D}(\lambda,295)}\times\frac{\sigma_{\mathrm{abs}}(\lambda,295)}{\sigma_{\mathrm{abs}}(\lambda,T)}\times\frac{T}{295}. \quad (7)$$

The first term simply references the measured signal to the $\Phi_{1D}(\lambda,295)$ value determined from Fig. 1. $S_{1D}(\lambda,295)$ is the measured signal at 295 K. In practice, this correction term was only significant for the two data sets taken at the longest wavelengths (Fig. 8). The third term reflects the temperature dependence of the parents' absorption at wavelength λ,[20] and the final term allows for the fact that we take measurements at constant *pressure* whilst the relevant quantity is the number density which, if we assume ideal gas behavior, will scale inversely with temperature. $\Phi_{1D}(\lambda,295)$ in Eq. (7) was set to the result obtained by the PHOFEX measurement in this study, as shown Fig. 5.

The filled points in Fig. 7 were obtained by monitoring the $O(^3P_2)$ atom yield at the chosen wavelengths, as a function of temperature, correcting for the temperature dependence of the parent number density and absorption cross-section as in Eq. (7), referencing to the relevant $\Phi_{3P}(\lambda,295)$ value derived from Fig. 5 and plotting the result as $(1-\Phi_{3P})$ vs T. Such an analysis is valid given that we have already established that the $O(^3P_j)$ spin–orbit branching ratio and the lineshape of the $O(3s\ ^3S^0-2p\ ^3P_2)$ probe transition are insensitive to both λ and T over the ranges relevant to Fig. 7. The match between these complementary data sets for $\lambda_{\mathrm{phot}}=308$, 310 and 312 nm is reassuringly good, as is the agreement between the present 308 nm data and the recent $\Phi_{1D}(T)$ measurements reported by Talukdar *et al.*[19] The present measurements also agree tolerably with the $\Phi_{1D}(\lambda,T)$ model currently recommended by NASA/JPL (dashed lines in Fig. 7) for wavelengths $\lambda_{\mathrm{phot}}=305$ and 312 nm,[2] but the agreement with the JPL/NASA recommendations[2] leaves a lot to be desired for $\lambda_{\mathrm{phot}}=308$, 310, 318 and 324.85 nm. Especially for $\lambda_{\mathrm{phot}}\geqslant 318$ nm the discrepancy between our data and the NASA/JPL recommendation is clearly large. This discrepancy is discussed later with relation to the high-resolution Doppler profile of the nascent $O(^1D)$ photofragments. Figures 7 and 8 show Φ_{1D} to be temperature independent both at the shortest and longest wavelengths, indicating that the $O(^1D)$ atoms produced at these wavelengths result almost entirely from excitation of O_3 molecules in their ground $(v''=0)$ state. The

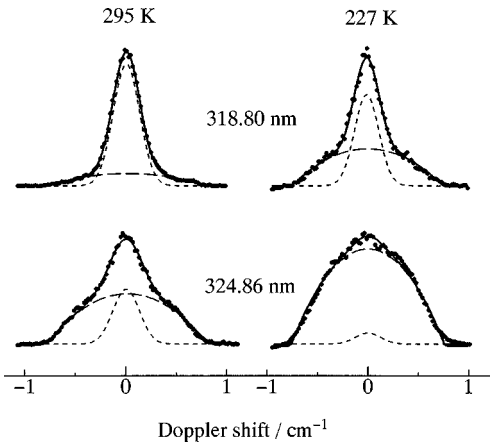

FIG. 9. High resolution Doppler profiles for the nascent $O(^1D)$ atoms generated from the photodissociation of ozone at: 318.80 nm and 295 K (top left); 324.85 nm and 295 K (bottom left); 318.80 nm and 227 K (top right); and 324.85 nm and 227 K (bottom left). An intracavity etalon was installed in the dye laser used to generate the necessary vuv probe radiation (linewidth ~ 0.2 cm^{-1}). The photolysis laser and vuv probe laser radiation counterpropagate through the reaction chamber. The pressure of ozone in the reaction cell was 4 mTorr and the photolysis—probe time delay was 60 ns. The observed Doppler profiles are shown as dots, while the solid lines represent the curves obtained by fitting the superposition of a wide component (broken line) corresponding to channel (2) and a narrow component (dotted line) corresponding to channel (1)—see the text for further details.

Φ_{1D} curves at intermediate λ_{phot} fall off with decreasing T, most notably at $\lambda_{\mathrm{phot}}=312$ and 318 nm, where Φ_{1D} declines by ~ 2.5 on cooling from 295 to 227 K. Such results provide further strong support for the idea that much of the $O(^1D)$ yield observed at these excitation wavelengths results from photolysis of internally excited parent molecules.

C. High-resolution Doppler profiles of the nascent $O(^1D)$ photoproducts

We measured the high resolution Doppler profiles of the nascent $O(^1D)$ photofragments from ozone at various photolysis wavelengths, scanning the vuv probe laser wavelength around 115.22 nm with an intracavity etalon. The linewidth of the etalon narrowed probe laser was ~ 0.2 cm^{-1}, as estimated from Doppler measurements of thermalized $O(^1D)$ atoms. Figure 9 shows the Doppler profiles of the nascent $O(^1D)$ atoms from ozone at photolysis wavelengths of 318.80 and 324.85 nm at 295 and 227 K, respectively. Both these wavelengths are beyond the long wavelength threshold for channel (1). The measured Doppler profiles consist of two components, one much wider than the other, as shown in Fig. 9. As indicated in our previous jet-cooled study,[11] the wide component comes from the spin-forbidden process leading to $O(^1D)+O_2(X\ ^3\Sigma_g^-)$ products [channel (2)]. The width simply indicates that the large excess energy associated with dissociation channel (2) permits production of fast $O(^1D)$ atoms. The narrow component is attributable to the spin-allowed process leading to formation of $O(^1D)+O_2(a\ ^1\Delta_g)$ products [channel (1)] following parent hot band excitation; its narrowness reflects the very small excess energy associated with the spin-allowed excitation process at this excitation wavelength. Figure 9 demonstrates the increased relative contribution of the wider component at

Downloaded 18 Oct 2006 to 133.6.32.11. Redistribution subject to AIP license or copyright, see http://jcp.aip.org/jcp/copyright.jsp

TABLE II. Absolute channel branching for the processes (1) and (2) in the uv photodissociation of O_3 derived from analysis of the high resolution Doppler profiles and the PHOFEX spectra of the $O(^1D)$ photofragments.

T (K)	λ_{phot} (nm)	Relative branching[a] $\Phi_{1D}^{SA}(\lambda,T)/\Phi_{1D}^{SF}(\lambda,T)$	$\Phi_{1D}^{total}(\lambda,T)$[b]	$\Phi_{1D}^{SF}(\lambda,T)$[c]	$\Phi_{1D}^{SA}(\lambda,T)$	$\Phi_{1D}^{SF}(\lambda,T)/[1-\Phi_{1D}^{SA}(\lambda,T)]$[d]
295	318.80	2.80±0.28	0.250±0.038	0.066±0.005	0.184±0.028	0.081±0.007
	319.36	2.52±0.24	0.230±0.035	0.065±0.005	0.165±0.025	0.078±0.006
	320.05	1.99±0.42	0.200±0.030	0.067±0.014	0.133±0.017	0.077±0.016
	321.00	1.56±0.59	0.195±0.029	0.076±0.010	0.119±0.017	0.086±0.011
	322.00	0.85±0.11	0.150±0.023	0.081±0.017	0.069±0.010	0.087±0.018
	322.71	0.46±0.03	0.120±0.018	0.082±0.009	0.038±0.006	0.085±0.009
	323.80	0.69±0.08	0.140±0.021	0.083±0.015	0.057±0.008	0.088±0.016
	324.86	0.24±0.03	0.100±0.015	0.080±0.029	0.020±0.002	0.082±0.029
	325.28	0.23±0.06	0.090±0.014	0.073±0.011	0.017±0.003	0.074±0.011
	325.54	0.20±0.03	0.095±0.014	0.079±0.007	0.016±0.002	0.080±0.007
	327.50	0.22±0.03	0.105±0.016	0.086±0.017	0.019±0.003	0.088±0.017
	327.99	0.13±0.03	0.090±0.014	0.080±0.023	0.010±0.002	0.081±0.023
227	318.80	0.66±0.06	0.105±0.016	0.063±0.010	0.042±0.006	0.066±0.011
	322.71	0.02±0.02	0.095±0.015	0.093±0.014	0.002±0.001	0.093±0.014
	324.86	0.01±0.01	0.095±0.014	0.094±0.013	0.001±0.001	0.094±0.013

[a]Channel branching for channels (1) and (2) obtained by fitting the narrow and wide components apparent in the $O(^1D)$ Doppler profiles (see the text). $\Phi_{1D}^{SA}(\lambda,T)$ and $\Phi_{1D}^{SF}(\lambda,T)$ are the $O(^1D)$ quantum yields via the spin-allowed (SA) and spin-forbidden (SF) processes, respectively, at photolysis wavelength λ and at temperature T.

[b]Total $O(^1D)$ quantum yield at λ and at T, which is obtained from the PHOFEX spectra measurements (Figs. 5 and 6).

[c]Calculated from the channel branching and the total $O(^1D)$ quantum yield, using the relation of $\Phi_{1D}^{TOTAL}(\lambda,T)=\Phi_{1D}^{SF}(\lambda,T)+\Phi_{1D}^{SA}(\lambda,T)$.

[d]Channel branching to the triplet surface at the crossing point on the **R** surface with the triplet surface correlating to channel (2) (see the text and Fig. 11).

the longer photolysis wavelength and at the lower temperature. Each Doppler profile in Fig. 9 contains contributions from the wide (broken curve) and narrow (dotted curve) components. Their relative contributions to each Doppler profile were calculated by a least square fitting procedure, so that the sum spectrum (solid curve) reproduced the experimentally obtained profile. In the fitting procedures, the shapes of the narrow and wide components were assumed to be independent of the photolysis wavelength and temperature. This approximation is justified by realising that the shape for the spin-allowed process (narrow component) is determined largely by the laser linewidth, whilst the Doppler width associated with the spin-forbidden contribution (wide component) is likely to be little changed given that the available energy for process (2) changes by only ~13% over the photolysis wavelength range used. All measured Doppler profiles were well reproduced by this fitting procedure, thus allowing estimation of the branching between channels (1) and (2) at a range of excitation wavelengths in the range of 318.80–327.99 nm at both 295 and 227 K (Table II). The branching ratio uncertainties quoted in Table II are the standard deviations returned in the fitting procedure. Given the total $O(^1D)$ quantum yields, Φ_{1D}^{Total}, obtained from analysis of the PHOFEX spectra (also listed in Table II) it is thus possible to calculate the $O(^1D)$ quantum yields from the spin-forbidden and spin-allowed channels (Φ_{1D}^{SF} and Φ_{1D}^{SA}, respectively) at each excitation wavelength from the relation

$$\Phi_{1D}^{Total}=\Phi_{1D}^{SF}+\Phi_{1D}^{SA}. \quad (8)$$

The ''partial'' quantum yields so obtained are also listed in Table II. We note that the quantum yields for the spin-forbidden channel (2) are almost independent of both photolysis wavelength and temperature.

IV. DISCUSSION

A. Model of the photodissociation processes of ozone

A reasonable consensus is now beginning to emerge as to the detailed form of the $O(^1D)$ quantum yield versus wavelength curve, its temperature dependence and, at least qualitatively, the explanation for the observed behavior. Numerous previous studies indicate an approximately constant $O(^1D)$ quantum yield for O_3 photodissociation at wavelengths $\lambda_{phot}\leqslant 305$ nm, with $\Phi_{1D}\sim 0.9-0.95$.[2] The present work suggests that at $\lambda_{phot}=305$ nm the value is at the low end of this range. The energy threshold for the spin allowed fragmentation channel (1) corresponds to $\lambda_{phot}=310.2\pm0.2$ nm.[12] The Φ_{1D} value declines as this wavelength is approached but remains greater than zero right out to $\lambda_{phot}=329$ nm (Figs. 5 and 6) and even to 336 nm.[14] It is the precise behavior in this long wavelength region, and its explanation, that is the topic of current concern.

The data shown in Figs. 5, 6, and 7 serve to reinforce the conclusion that spin-allowed [channel (1)] photodissociation of internally excited ozone molecules makes a significant contribution to the $O(^1D)$ quantum yield at $\lambda_{phot}>310$ nm. Clearly, the pedestal in the 310–320 nm part of the $O(^1D)$

Downloaded 18 Oct 2006 to 133.6.32.11. Redistribution subject to AIP license or copyright, see http://jcp.aip.org/jcp/copyright.jsp

yield curve is more evident at 295 K than at 227 K (Figs. 5 and 6), or under molecular beam conditions.[11,12] This pedestal is associated with the spin-allowed photodissociation of vibrationally excited ozone molecules.[11,12] Such an interpretation is supported by the temperature dependence of the Φ_{1D} curves shown in Figs. 7 and 8, by the form of the PHOFEX spectra for forming both $O(^1D)$ atoms[12] and the $O_2(a\ ^1\Delta_g)$ copartners,[5,8] by measurements of the recoil kinetic energies of the latter[9] and by modelling studies.[16]

Furthermore, in the results section, we have provided clear evidence that the spin-forbidden dissociation process (2) contributes to the formation of $O(^1D)$ atoms at long wavelengths. As Figs. 5 and 6 demonstrate, the current NASA/JPL recommendations for use in stratospheric modeling still underestimate the $O(^1D)$ quantum yield from O_3 photolysis at $\lambda_{phot}>320$ nm. Figure 8 shows Φ_{1D} to be almost temperature independent at $\lambda_{phot}=324.86$ nm, implying that the bulk of the measured $O(^1D)$ atoms arise from photolysis of ground state O_3 molecules. Energetic considerations then dictate that these fast fragments can only arise via the spin-forbidden channel (2). Jet-cooled studies[11,12] show that the fastest $O(^1D)$ atoms arise when exciting within vibronic absorption bands associated with the Huggins system, and exhibit maximum Doppler shifts fully consistent with fragmentation via channel (2). With warmer samples, the attendant rotational congestion leads to some Huggins band contribution to the absorption at all of these long wavelengths. The measured Doppler profiles of the photofragment $O(^1D)$ atoms in Fig. 9 demonstrate the dominant role of the spin-forbidden process (2) as the source of the $O(^1D)$ atoms observed at the long photodissociation wavelengths. The results shown in Table II indicate that the $O(^1D)$ production yield via the spin-forbidden $O(^1D)+O_2(X\ ^3\Sigma_g^-)$ channel has almost constant value ($\Phi_{1D}^{SF}\sim 0.07-0.08$) over the photodissociation wavelength ranges of 318–329 nm and is almost independent of the gas temperature.

Figure 10 shows schematic sections through potential energy surfaces (PESs) that can provide a rationale for the photoexcitation and dissociation processes of ozone at photolysis wavelengths $\lambda_{phot}\sim 310$ nm. These potential curves are taken from Ref. 23, except for the triplet curves correlating to the spin-forbidden channels. The number and nature of the excited electronic states of ozone reached by one photon excitation in this wavelength range remains the subject of some controversy. The strong absorption centered at ~ 250 nm, the Hartley band, extends into this wavelength range. The Hartley band has been assigned unambiguously to the strongly allowed $^1B_2-X\ ^1A_1$ transition. The vibronic structure evident in the absorption spectrum of O_3 at $\lambda>310$ nm is traditionally referred to as the Huggins band system. The literature contains two possible interpretations for the Huggins system: (a) absorption to weakly bound states supported in the shallow minima in the $O-O_2$ exit channels of the excited $^1B_2$ PES, lying below the dissociation limit to $O(^1D)+O_2(a\ ^1\Delta_g)$[17,24–26] and (b) transitions to the $2\ ^1A_1$ electronic state. The observed weakness of the Huggins system in the former interpretation is ascribed to small Franck–Condon factors whilst, in the latter case, it is attributable to the orbitally forbidden nature of the

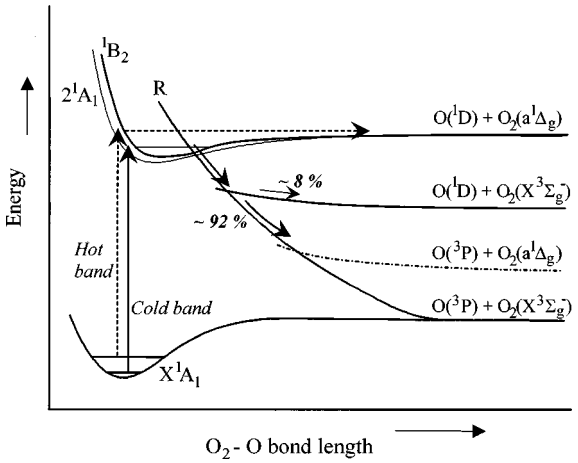

FIG. 10. Schematic diagram of the model for the photoexcitation and dissociation processes of O_3 at the wavelength range $\lambda_{phot}>310$ nm with sectional curves of low-lying potential energy surfaces of O_3 along the dissociation coordinate $R(O_2-O)$. The potential curves are taken from the Ref. 23, except for the triplet curves correlating to the spin-forbidden channels. Symmetry representations are in C_{2v} point group. $O(^1D)$ formation via hot band excitation followed by spin-allowed dissociation [channel (1)] is indicated by the broken lines and arrows, while the $O(^1D)$ and $O(^3P)$ formation processes following excitation of vibrationless ozone molecules are indicated by solid lines and arrows (see the text).

$2\ ^1A_1-X\ ^1A_1$ one photon transition.[12,18,27–29] Hot band excitation to the repulsive limb of the excited $^1B_2$ (and/or $2\ ^1A_1$) state above the dissociation limit for the spin-allowed process (1) results in rapid dissociation to $O(^1D)+O_2(a\ ^1\Delta_g)$ products. Such hot band excitation is indicated by the broken arrows in Fig. 10. Excitation of ground state $O_3(X\ ^1A_1, v''=0)$ molecules at photolysis wavelengths $\lambda>310$ nm cannot exceed the energetic threshold for $O(^1D)+O_2(a\ ^1\Delta_g)$ production and thus these molecules predissociate predominantly to $O(^3P)+O_2(X\ ^3\Sigma_g^-)$ fragments [channel (4)], following surface crossing from the photoprepared $^1B_2$ (and/or $2\ ^1A_1$) state to a repulsive state (labelled **R**).[23] The latter process is indicated by the solid arrows in Fig. 10. The yield of ozone molecules undergoing radiationless transfer from the initially prepared $^1B_2$ (and/or $2\ ^1A_1$) state to the **R** repulsive state can be expressed as $(1-\Phi_{1D}^{SA})$. The $O(^1D)$ PHOFEX spectrum obtained following excitation in the wavelength range $\lambda_{phot}>320$ nm at 227 K (Fig. 2) and in the previous jet-cooled studies[11] is seen to mimic the vibrational structure evident in the parent absorption spectrum. The dominant dissociation process at these wavelengths involves formation of $O(^3P)+O_2(X\ ^3\Sigma_g^-)$ products [channel (4)] whilst the minor yield of $O(^1D)$ atoms arise mainly via the spin-forbidden channel (2). These facts strongly suggest that the spin-allowed $O(^3P)+O_2(X\ ^3\Sigma_g^-)$ products [channel (4)] and the spin-forbidden $O(^1D)+O_2(X\ ^3\Sigma_g^-)$ products [channel (2)] originate from the *same* photoexcited state ($^1B_2$ and/or $2\ ^1A_1$) of the parent, and that it is unnecessary to invoke any direct excitation to a parent triplet state to account for the observed 'spin-forbidden' product yield. Thus, in the spirit of Fig. 10, we propose that the spin-forbidden products arise as a result of (i) coupling from the $^1B_2/2\ ^1A_1$ state to the **R** state potential and (ii) a subsequent intersystem crossing (ISC) from the **R** state to the triplet surface corre-

Downloaded 18 Oct 2006 to 133.6.32.11. Redistribution subject to AIP license or copyright, see http://jcp.aip.org/jcp/copyright.jsp

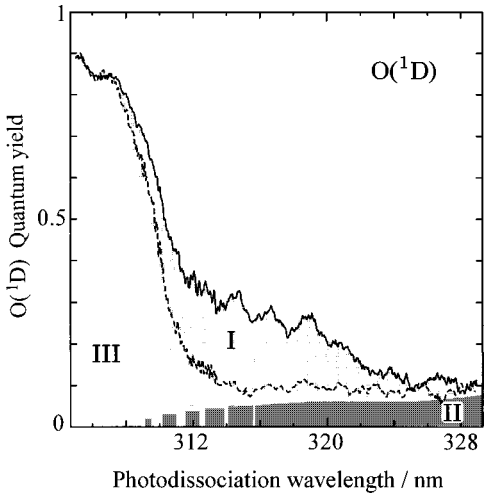

FIG. 11. Schematic diagram depicting the contributions made by the various dissociation processes contributing to the quantum yield spectra for $O(^1D)$ atoms from O_3 photolysis in the wavelength range 305–329 nm. The solid curve is the quantum yield spectrum obtained experimentally at 295 K (Fig. 5), while the broken curve is that obtained at 227 K (Fig. 6). Region I (shaded) indicates the contribution from the hot band excitation process leading to $O(^1D)$ formation via channel (1) at 295 K, region II (black) represents the contribution from the spin-forbidden process leading to $O(^1D)$ formation via channel (2), whilst region III corresponds to the $O(^1D)$ formation following excitation of parent $v''=0$ molecules and dissociation via channel (1).

lating with the products $O(^1D)+O_2(X\ ^3\Sigma_g^-)$. We can define the following branching ratios in this latter crossing region: $\Phi_{3P}^{\mathrm{TOTAL}}/(1-\Phi_{1D}^{\mathrm{SA}})$ and $\Phi_{1D}^{\mathrm{SF}}/(1-\Phi_{1D}^{\mathrm{SA}})$ describing, respectively, that fraction of the dissociating molecules that remain on the **R** surface and yield $O(^3P)$ atoms via channel (3) and/or (4) and the fraction that transfer to the triplet surface and fragment via channel (2). These branching ratios can be calculated from the present experimental results. Table II shows that the values of $\Phi_{1D}^{\mathrm{SF}}/(1-\Phi_{1D}^{\mathrm{SA}})$ so derived are consistently in the range of 0.08 ± 0.01, with no discernible dependence upon the precise photolysis wavelength or the gas temperature. Thus we conclude that, for all investigated photolysis wavelengths $\lambda_{\mathrm{phot}}>318$ nm, ~8% of the dissociating molecules 'cross' from the **R** state to the triplet state surface and dissociate via channel (2).

Figure 11 depicts schematically the contributions that the various possible dissociation processes make to the measured $O(^1D)$ quantum yield spectrum in the wavelength range 305–329 nm. Region I in Fig. 11 indicates the contribution that hot band excitation and dissociation via channel (1) makes to the $O(^1D)$ yield at 295 K, whilst region II illustrates the wavelength dependence of the spin-forbidden process resulting in $O(^1D)$ formation via channel (2). The approximate partitioning of regions I and II is indicated in Fig. 11. Region III corresponds to $O(^1D)$ formation via channel (1) following excitation of O_3 molecules in their ground vibrational level. Clearly, the spin-forbidden [channel (2)] contribution to the overall $O(^1D)$ quantum yield becomes progressively less important as we move to shorter excitation wavelengths but, in the long wavelength region ($\lambda_{\mathrm{phot}}>325$ nm), it is the dominant route to $O(^1D)$ formation. It seems reasonable that $O(^1D)$ production via the spin-forbidden process continues to still longer photolysis wavelengths than those studied here with a similar (i.e., ~8%) yield, though we also recognise that the absorption cross-section of ozone becomes very small at these wavelengths. Conversely, at the short wavelength limit we suspect that the relative contribution from the spin-forbidden $O(^1D)$ formation route decreases rapidly and becomes negligible at wavelengths $\lambda_{\mathrm{phot}}<310$ nm, because the rate of radiationless transfer to the **R** state and, subsequently, to the triplet surface is unable to compete with the fast direct photodissociation to singlet products above the threshold for channel (1).

In the lower stratosphere and troposphere of the Earth, $O(^1D)$ atoms produced via channels (1) and (2) can undergo reaction with water vapor in the atmosphere to form OH radicals, the most important oxidizing agent for many species.[16] Thus, both for our understanding of the chemical processes occurring in the Earth's atmosphere and for establishing its oxidative capacity, it is important to determine accurately the wavelength and temperature dependence of the $O(^1D)$ yield arising from the photodissociation of O_3. The present results indicate that the current NASA/JPL recommendations[2] still underestimate the $O(^1D)$ quantum yield from ozone photolysis at the longer wavelengths, especially at $\lambda_{\mathrm{phot}}>320$ nm where we show that the $O(^1D)$ quantum yield has almost no dependence upon either temperature or photolysis wavelength—findings that are understandable once we have shown [by Doppler line shape measurements and by studies of the temperature dependence of the $O(^1D)$ yield] that the dominant route to $O(^1D)$ formation at these longer wavelengths is the spin-forbidden process (2). The deduced greater than hitherto assumed $O(^1D)$ yield from O_3 photolysis at $\lambda_{\mathrm{phot}}>320$ nm will likely have particular significance for photochemistry in the atmosphere at high solar zenith angle and at lower temperatures.

B. Quantitative analysis of the $O(^1D)$ quantum yield from ozone photolysis

The temperature dependence of the $O(^1D)$ atom formation from ozone photolysis can be simulated using the photodissociation model proposed above. The PHOFEX spectrum of $O(^1D)$ from ozone photolysis under jet-cooled conditions revealed two appearance threshold wavelengths for the $O(^1D)$ formation processes.[12] The two threshold wavelengths were interpreted in terms of excitation of ground state O_3 molecules, at 310 ± 0.2 nm, and to a hot band excitation, at 320.7 ± 0.2 nm. The energy difference between these two threshold wavelengths accords well with the antisymmetric stretching fundamental frequency in the $X\ ^1A_1$ state ($\nu_3=1042\ \mathrm{cm}^{-1}$). Thus it was concluded that population in the $v_3''=1$ level of the ground state makes the main contribution to the hot band excitation. The fractional population in the $v_3''=1$ vibrational level at temperature T is expressed by a Boltzmann factor

$$f(\nu_3''=1,T)=\frac{\exp\left[-\dfrac{E(\nu_3''=1)}{kT}\right]}{\sum\ \exp\left[-\dfrac{E(\nu'')}{kT}\right]}\simeq\exp\left[-\frac{E(\nu_3''=1)}{kT}\right], \quad (9)$$

Downloaded 18 Oct 2006 to 133.6.32.11. Redistribution subject to AIP license or copyright, see http://jcp.aip.org/jcp/copyright.jsp

where k is the Boltzmann constant and we use the condition $E(v'') \gg kT$ for all vibrational states. From Eq. (9) we can deduce that $f(v_3''=1,\ 227\ \mathrm{K}) = 1.35\times10^{-3}$ and $f(v_3''=1,\ 295\ \mathrm{K}) = 6.19\times10^{-3}$. Even at 295 K, the fractional population in the $v_3''=1$ level is very small, although the contribution that hot band excitation makes to the $O(^1D)$ quantum yield spectrum is large (Fig. 11). This large contribution is explicable in terms of the Franck–Condon factor for optical excitation from the $v_3''=1$ level at these wavelengths being 10 to 100 times larger than that for excitation from the zero-point level.[11,12,16] The ratio of the relative populations in the $v_3''=1$ level at 227 K and 295 K is $f(v_3''=1,\ 227\ \mathrm{K})/f(v_3''=1,\ 295\ \mathrm{K}) = 0.22$. This is entirely consistent with the present measurements of the temperature dependent $O(^1D)$ quantum yields at $\lambda_{\mathrm{phot}}=318.80$ nm, viz. $\Phi_{1D}^{\mathrm{SA}}(227\ \mathrm{K})/\Phi_{1D}^{\mathrm{SA}}(295\ \mathrm{K}) = 0.23$ (see Table II), and reinforces our conclusion that hot band excitation and dissociation via the spin-allowed channel (1) is the dominant source of $O(^1D)$ atoms at this photolysis wavelength. Moving to longer wavelengths, e.g., 322.71 or 324.86 nm, the only spin-allowed dissociation route to $O(^1D)$ atoms should involve hot band excitation from the $v_3''=2$ level of $O_3(X\ ^1A_1)$. The measured contributions attributable to the spin-allowed channel (1) at both of these wavelengths, at 227 and 295 K, are in the ratio $\Phi_{1D}^{\mathrm{SA}}(227\ \mathrm{K})/\Phi_{1D}^{\mathrm{SA}}(295\ \mathrm{K}) \approx 0.04$ (see Table II) which is in excellent agreement with the expected Boltzmann factor of $0.22^2 \approx 0.04$.

We now proceed to parameterize the measured wavelength and temperature dependence of the $O(^1D)$ quantum yield from ozone photolysis based on the model proposed in Sec. IV A. The total quantum yield for $O(^1D)$ formation at photolysis wavelength λ at temperature T, $\Phi_{1D}^{\mathrm{TOTAL}}(\lambda,T)$, is expressed by the following simple equation with reference to the value of the $O(^1D)$ quantum yield at 295 K;

$$\begin{aligned}\Phi_{1D}^{\mathrm{TOTAL}}(\lambda,T) &= \Phi_{1D}^{\mathrm{SF}}(\lambda,T) + \Phi_{1D}^{\mathrm{SA}}(\lambda,T)\\ &= 0.08[1-\Phi_{1D}^{\mathrm{SA}}(\lambda,T)] + \Phi_{1D}^{\mathrm{SA}}(\lambda,T)\\ &= 0.08 + 0.92[\Phi_{1D}^{\mathrm{COLD}}(\lambda,T) + \Phi_{1D}^{\mathrm{HOT}}(\lambda,T)]\\ &= 0.08 + 0.92\cdot\Phi_{1D}^{\mathrm{COLD}}(\lambda,T)\\ &\quad + 0.92\cdot\Phi_{1D}^{\mathrm{HOT}}(\lambda,295)\cdot f(v,T)/f(v,295),\end{aligned} \tag{10}$$

where $\Phi_{1D}^{\mathrm{SF}}(\lambda,T)$ and $\Phi_{1D}^{\mathrm{SA}}(\lambda,T)$ are $O(^1D)$ quantum yields arising from the spin-forbidden [channel (2)] and spin-allowed [channel (1)] processes, respectively, and $\Phi_{1D}^{\mathrm{COLD}}(\lambda,T)$ and $\Phi_{1D}^{\mathrm{HOT}}(\lambda,T)$ are the $O(^1D)$ quantum yields for the spin-allowed dissociation via channel (1) following $v''=0$ and $v''>0$ excitation processes, respectively. This model implies a slight temperature and wavelength dependence for the contribution made by the spin-forbidden process (2). Figure 12 illustrates how well this parametrization [Eq. (10)] reproduces the temperature dependent $O(^1D)$ quantum yields measured at the photolysis wavelengths of 312, 318, and 324.86 nm. The simulations use the present $O(^1D)$ quantum yields experimentally obtained at 295 K at each excitation wavelength as the reference values. Since all three photolysis wavelengths are longer than 310.2 nm, the threshold wavelength for $O_3(v''=0)$ molecules to dissociate via channel (1), the contribution of $\Phi_{1D}^{\mathrm{COLD}}(\lambda,T)$ was ignored in the simulation. The simulated quantum yields (smooth curves) agree well with the present experimental data (open and closed circles) within the experimental errors. Regions I and II beneath the total $O(^1D)$ quantum yield curve (broken line) in each panel of Fig. 12 indicates the absolute contribution made by hot band excitation followed by spin-allowed dissociation via channel (1), and by spin-forbidden dissociation [channel (2)], respectively. Clearly, the measured temperature dependence of the $O(^1D)$ quantum yield can be explained most satisfactorily in terms of the dissociation model described in Sec. IV A.

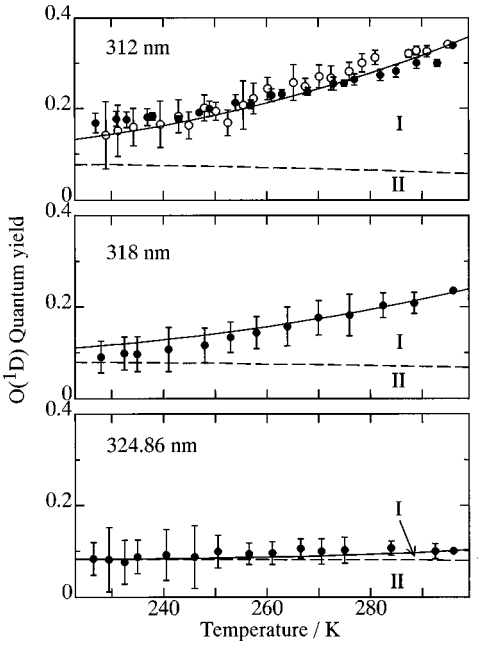

FIG. 12. Plots comparing the experimentally derived temperature dependence of the $O(^1D)$ quantum yields measured at photolysis wavelengths of 312, 318, and 324.86 nm (as shown in Figs. 7 and 8) with the results of simulations using Eq. (10) (smooth curves—see the text for further details).

V. CONCLUSION

Both $O(^1D)$ and $O(^3P_j)$ atom photoproducts from the uv photodissociation of ozone have been detected directly using the technique of vacuum ultraviolet laser induced fluorescence at wavelengths around 115 and 130 nm, respectively. The photofragment excitation (PHOFEX) spectra for both $O(^1D)$ and $O(^3P)$ atoms were recorded by monitoring the respective vuv-LIF signals while scanning the photodissociation wavelength between 305 and 329 nm. Very careful analysis of these PHOFEX spectra permits determination of the wavelength dependence of the absolute $O(^1D)$ production yield from the uv photodissociation of ozone at both 295 and 227 K. The detailed temperature dependence of the $O(^1D)$ yield throughout the range 227–295 K has been investigated at a number of photolysis wavelengths within this range. Comparison between the present results and the most recent recommendations by NASA/JPL for the wavelength and temperature dependence of the $O(^1D)$ yield from O_3 photolysis highlights remaining deficiencies in the recom-

Downloaded 18 Oct 2006 to 133.6.32.11. Redistribution subject to AIP license or copyright, see http://jcp.aip.org/jcp/copyright.jsp

mendations at the longer photodissociation wavelengths ($\lambda_{phot}>318$ nm). These discrepancies are attributable to contributions from the $O(^1D)$ atoms generated via the spin-forbidden $O(^1D)+O_2(X\ ^3\Sigma_g^-)$ product channel, which is not included in the current NASA/JPL recommendation. The importance of this spin-forbidden channel (2), as a source of $O(^1D)$ atoms, was confirmed by high resolution Doppler line shape measurements of nascent $O(^1D)$ photoproducts produced at these longer excitation wavelengths and by investigating the temperature dependence of $O(^1D)$ product formation at $\lambda_{phot}>318$ nm. At still longer photolysis wavelengths (e.g., $\lambda_{phot}=325$ nm the $O(^1D)$) yield shows negligible temperature dependence. It is well known that $O(^1D)$ atoms produced from the ultraviolet photodissociation of O_3 have a key role in determining the oxidizing capacity of the troposphere and lower stratosphere and the ensuing photochemistry occurring in these regions of the atmosphere. $O(^1D)$ atoms formed at longer photolysis wavelengths will make a significant contribution in photodissociation processes at larger solar zenith angle and at lower temperatures, because of this finding that the $O(^1D)$ yield at longer wavelength is almost independent of both the temperature and the photodissociation wavelength. The absolute quantum yield for $O(^1D)$ production via the spin-forbidden channel (2) was estimated to be ~ 0.08 at $\lambda_{phot}>318$ nm from analyses of the high resolution $O(^1D)$ atom Doppler profiles. Clearly further work is required to provide a physical interpretation of the factors controlling the branching into the various possible fragmentation channels following excitation of O_3 within its Huggins band system. Such insight could derive from further theoretical calculations which include possible singlet–triplet interactions after the initial photoexcitation process as well as from experimental studies of the internal energy and kinetic energy distributions of the photoproducts arising in the Huggins band photodissociation of O_3.

ACKNOWLEDGMENTS

This work is partly supported by a Grant-in-Aid for Scientific Research from the Ministry of Education, Science, and Culture of Japan (Y.M.). The Heiwa-Nakajima Foundation (M.K.) and the Daiko Foundation (Y.M.) are also acknowledged for financial support. M.K. and M.N.R.A. are grateful to the British Council, the Royal Society and the Japan Society for support under the Japan–UK Cooperative Program. The authors thank Professor A. R. Ravishankara and Professor G. Hancock for their helpful discussions.

[1] H. Okabe, *Photochemistry of Small Molecules* (Wiley Interscience, New York, 1978).
[2] W. B. DeMore, S. P. Sander, D. M. Golden, R. F. Hampson, M. J. Kurylo, C. J. Howard, A. R. Ravishankara, C. E. Kolb, and M. J. Molina, *Chemical Kinetics and Photochemical Data for use in Stratospheric Modelling, Evaluation No. 12*, JPL Publication 97-4 (1997), and references therein.
[3] M. Trolier and J. R. Wiesenfeld, J. Geophys. Res. **93**, 7119 (1988).
[4] J. C. Brock and R. T. Watson, Chem. Phys. **46**, 477 (1980).
[5] S. M. Ball, G. Hancock, I. J. Murphy, and S. P. Rayner, Geophys. Res. Lett. **20**, 2063 (1993).
[6] S. M. Shamsuddin, Y. Inagaki, Y. Matsumi, and M. Kawasaki, Can. J. Chem. **72**, 637 (1993).
[7] S. M. Ball, G. Hancock, and F. Winterbottom, Faraday Discuss. Chem. Soc. **100**, 215 (1995).
[8] S. M. Ball and G. Hancock, Geophys. Res. Lett. **22**, 1213 (1995).
[9] S. M. Ball, G. Hancock, J. C. Pinot de Moira, C. M. Sadowski, and F. Winterbottom, Chem. Phys. Lett. **245**, 1 (1995).
[10] K. Takahashi, Y. Matsumi, and M. Kawasaki, J. Phys. Chem. **100**, 4084 (1996).
[11] K. Takahashi, M. Kishigami, Y. Matsumi, M. Kawasaki, and A. J. Orr-Ewing, J. Chem. Phys. **105**, 5290 (1996).
[12] K. Takahashi, M. Kishigami, N. Taniguchi, Y. Matsumi, and M. Kawasaki, J. Chem. Phys. **106**, 6390 (1997).
[13] S. M. Ball, G. Hancock, S. E. Martin, and J. C. Pinot de Moira, Chem. Phys. Lett. **264**, 531 (1997).
[14] E. Silvente, R. C. Richter, M. Zheng, E. S. Saltzman, and A. J. Hynes, Chem. Phys. Lett. **264**, 309 (1997).
[15] R. K. Talukdar, M. K. Gilles, F. Battin-Leclerc, A. R. Ravishankara, J.-M. Fracheboud, J. J. Orlando, and G. S. Tyndall, Geophys. Res. Lett. **24**, 1091 (1997).
[16] H. A. Michelsen, R. J. Salawitch, P. O. Wennberg, and J. G. Anderson, Geophys. Res. Lett. **21**, 2227 (1994).
[17] D. H. Katayama, J. Chem. Phys. **71**, 815 (1979).
[18] J. A. Joens, J. Chem. Phys. **101**, 5431 (1994).
[19] L. T. Molina and M. J. Molina, J. Geophys. Res. **91**, 14501 (1986).
[20] J. Malicet, D. Daumont, J. Charbonnier, C. Parisse, A. Chakir, and J. Brion, J. Atmos. Chem. **21**, 263 (1995).
[21] S. Gerstenkorn and P. Luc, *Atlas du Spectre D'Absorption de la Molecule D'Iode* (C.N.R.S., Paris, 1978).
[22] R. Hilbig and R. Wallenstein, Appl. Opt. **21**, 913 (1982).
[23] P. J. Hay, R. T Pack, R. B. Walker, and E. J. Heller, J. Phys. Chem. **86**, 862 (1982).
[24] A. Sinha, D. Imre, J. H. Goble, Jr., and J. L. Kinsey, J. Chem. Phys. **84**, 6108 (1986).
[25] F. LeQuéré and C. Leforestiér, Chem. Phys. Lett. **189**, 537 (1992).
[26] O. Bludsky and P. Jensen, Mol. Phys. **91**, 653 (1997).
[27] J. C. Brand, K. J. Cross, and A. R. Hoy, Can. J. Chem. **56**, 327 (1978).
[28] A. Banichevich and S. D. Peyerimhoff, Chem. Phys. **174**, 93 (1993).
[29] A. Banichevich, S. D. Peyerimhoff, and F. Grein, Chem. Phys. **178**, 155 (1993).

Downloaded 18 Oct 2006 to 133.6.32.11. Redistribution subject to AIP license or copyright, see http://jcp.aip.org/jcp/copyright.jsp